Synthesis, Conformation, and Activity of HCO-Met-Δ^Z Leu-Phe-OMe, an Active Analogue of Chemotactic *N*-Formyltripeptides

G. PAGANI ZECCHINI,[1] M. PAGLIALUNGA PARADISI,[1] I. TORRINI,[1] G. LUCENTE,[1,*] E. GAVUZZO,[2] F. MAZZA,[2] G. POCHETTI,[2] M. PACI,[3] M. SETTE,[3] A. DI NOLA,[4] G. VEGLIA,[4] S. TRANIELLO,[5] and S. SPISANI[5]

[1]Dipartimento di Studi Farmaceutici and Centro di Studio per la Chimica del Farmaco del CNR, Università La Sapienza, 00185 Roma; [2]Istituto di Strutturistica Chimica G. Giacomello CNR, C.P. n. 10, 00016 Monterotondo Stazione, Roma; [3]Dipartimento di Scienze e Tecnologie Chimiche, Università di Roma, V. O. Raimondo, 00173 Roma; [4]Dipartimento di Chimica, Università La Sapienza, 00185 Roma; [5]Istituto di Chimica Biologica, Università di Ferrara, 44100 Ferrara, Italy

SYNOPSIS

In order to induce a β-turn conformation into the chemotactic linear tripeptide *N*-formyl-L-methionyl-L-leucyl-L-phenylalanine (fMLP), the new analogue *N*-formyl-L-methionyl-Δ^Zleucyl-L-phenylalanine methyl ester [Δ^ZLeu]^{2}fMLP-OMe (**1**) has been synthesized. The conformational and biochemical consequences of this chemical modification have been determined. Analogue **1** has been synthesized by using *N*-carboxy-(Z)-α,β-didehydroleucine anhydride as key compound to introduce the unsaturated residue at the central position of the tripeptide **1**. The x-ray analysis shows that **1** adopts in the crystal a type II β-turn conformation in which the new residue occupies the $(i+2)$ position, and an intramolecular H bond is formed between the formylic oxygen and the Phe NH. ^{1}H-nmr analysis based on nuclear Overhauser effect measurements suggests that the same folded conformation is preferred in $CDCl_3$ solution; this finding is also supported by molecular dynamics simulation. The biological activity of **1** has been determined on human neutrophils (polymorphonuclear leukocytes) and compared to that shown by fMLP-OMe. Chemotactic activity, granule enzyme release, and superoxide anion production have been determined. Analogue **1** is practically inactive as chemoattractant, highly active in the superoxide generation, and similar to the parent in the lysozyme release. The conformational restriction imposed on the backbone by the presence of the unsaturated residue is discussed in relation with the observed bioselectivity. © 1993 John Wiley & Sons, Inc.

INTRODUCTION

Neutrophil chemotactic factors are receiving increasing attention.[1] These compounds, which are of different origin, chemical nature, and molecular size, share in common the property of attracting neutrophils to the inflammatory sites (chemotaxis). Among the most potent chemoattractants is a family of *N*-formyl peptides, which are of microbial origin and possess specific receptors located on the neutrophil cell surface. The interaction of these ligands with their receptors induces not only chemotaxis but also a variety of cellular responses, among which are superoxide generation and lysosomal enzyme release.

The HCO-Met-Leu-Phe-OH (fMLP) is the most extensively studied molecule of this group of chemoattractants and well-established structure–activity relationships have been determined by using this molecular model.[2] More recent studies concern the role of the peptide backbone conformation on the activity, with particular attention focused on the selection of the various cellular responses by using conformationally constrained ligands.

As a part of a continuing program to investigate the conformation–activity relationship of chemotactic formyl peptides[3,4] and as a continuation of

Biopolymers, Vol. 33, 437–451 (1993)

CCC 0006-3525/93/030437-15

* To whom correspondence should be addressed.

our preliminary communication,[5] we report here the synthesis, conformation, and biological activity of the conformationally constrained fMLP analogue containing Δ^ZLeu at the central position, HCO-Met-Δ^ZLeu-Phe-OMe (1).

RESULTS AND DISCUSSION

Synthesis

Synthesis of **1** is reported in Scheme 1. The *N*-protected intermediate Boc-Met-Δ^ZLeu-Phe-OMe has been obtained by following the one-pot procedure of Shin[6] starting from *N*-carboxy-(Z)-α,β-didehydroleucine anhydride (Δ^ZLeu·NCA)[7]; this was treated in sequence with *N*-*t*-butyloxycarbonyl-L-methionine (Boc-Met-OH)/dicyclohexyl carbodiimide and L-phenylalanine methyl ester (H-Phe-OMe). Treatment of the Boc-protected tripeptide with formic acid followed by *N*-ethoxycarbonyl-2-ethoxy-1,2-dihydroquinoline (EEDQ) gave HCO-Met-Δ^ZLeu-Phe-OMe (**1**) without affecting the unsaturated residue.

X-ray Structure

Molecular Geometry. The valence bond lengths and angles involving the nonhydrogen atoms of HCO-Met-Δ^ZLeu-Phe-OMe together with the adopted numbering scheme are reported in Figure 1. Crystal data and final fractional coordinates of **1** are reported in Tables I and II, respectively. Although rather large estimated standard deviations (ESDs) affect them, especially when involving peripherical atoms, their values are comparable, within the limits of the experimental errors, to those reported in the literature for the same residues.

The side chain of the didehydroleucine residue adopts, as expected, Z geometry with the vinyl hydrogen atom on the same side of the adjacent carbonyl group.[8-12] The length of 1.32(2) Å of the C_2^α-C_2^β bond is in agreement with the average value of 1.323(2) Å quoted for this bond.[8] The planarity imposed by the α,β-double bond should promote an electronic delocalization with shrinking of the C^α-N and C^α-C′ bonds, and lengthening of the carbonyl double bond. The C_2^α-N_2 and C_2^α-C_2' lengths of 1.42(2) and 1.51(2) Å, respectively, are in accordance with the expected electronic effects, and with the mean values reported for this residue.[8] The C_2'-O_2 bond, on the other hand, seems only scarcely influenced by the electronic effects and presents a bond length of 1.21(2) Å, which is at the lowest limit of accordance with the weighted average value reported for the same bond (1.258 Å).[8] It should be noted, however, that values as short as 1.18(2) and 1.20(1) Å have been found in the crystal structure of Boc-Pro-Δ^ZLeu-OMe.[9] As a result of the unfavorable interactions between the Δ^ZLeu side chain and the neighboring backbone atoms, the involved N-C^α-C′, N-C^α-C^β, and C^α-C^β-C^γ angles deviate from the standard value of 120°; the corresponding values of 117.8(8)°, 124.9(9)°, and 126(1)°, found in the present structure, are in agreement with weighted average literature values of 116.9(1)°, 122.9(1)°, and 127.3(1)° observed for unsaturated residues.[8]

Conformation. A perspective view of the peptide conformation found in the crystal is shown in Figure 2. The relevant torsion angles computed according to Ref. 13 are reported in Table III. The peptide adopts in the crystal a type II β-turn conformation characterized by torsion angles: $\varphi_1 = -55(1)°$, $\psi_1 = 129.7(8)°$, $\varphi_2 = 72.2(9)°$, $\psi_2 = 14.3(8)°$, which are in agreement with those reported for the ideal type II β-bend: $\varphi_1 = -60°$, $\psi_1 = 120°$, $\varphi_2 = 80°$, $\psi_2 = 0°$.[8] Analogous β-bend conformations have been found in the crystals of Boc-Phe-Δ^ZLeu-Val-OMe,[10] and of Boc-Pro-Δ^ZLeu-NHMe.[11] As a result of the backbone turn, a weak 1–4 intramolecular hydrogen bond, 3.15(2) Å long, occurs between the formylic CO and the Phe NH groups. The φ and ψ of the Δ^ZLeu residue correspond to a minimum energy region of the conformational map of α,β-unsaturated amino acid derivatives.[14] It is worthwhile to observe that the present study reports the first crystallo-

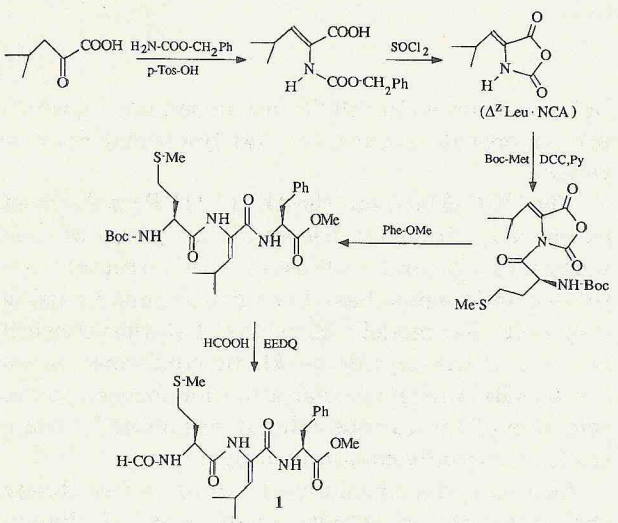

Scheme 1

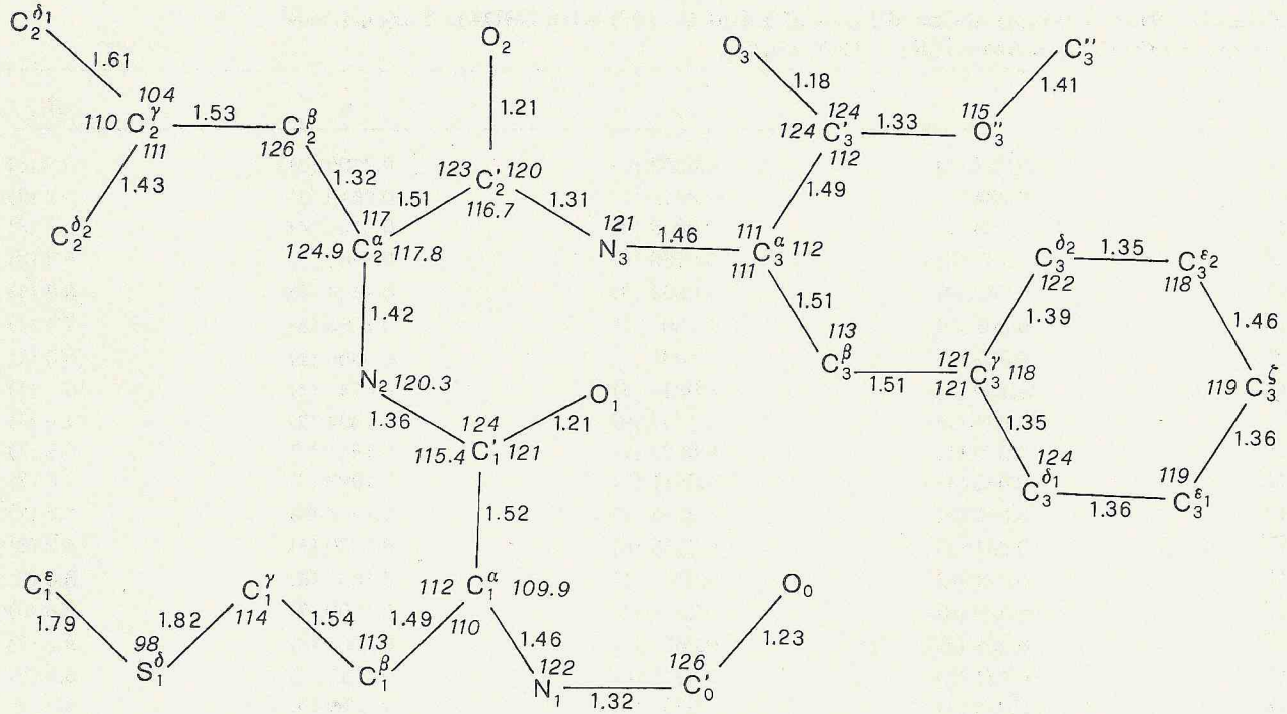

Figure 1. Atomic numbering scheme, valence bond lengths (Å) and angles (°) of HCO-Met-Δ^ZLeu-Phe-OMe (1). ESDs are in the range 0.01–0.03 Å and 0.7–1.4° for lengths and angles, respectively.

graphic analysis in which the formylic group is intramolecularly hydrogen-bonded to give a β-bend structure.

Table I Crytal Data for HCO-Met-Δ^ZLeu-Phe-OMe (1)

Molecular formula	$C_{22}H_{31}N_3O_5S \cdot \frac{1}{2} C_6H_6 \cdot H_2O$
Formula weight	506.6
Crystal system	Monoclinic
a	5.686 (3) Å
b	16.289 (15) Å
c	32.678 (23) Å
β	96.62 (5)°
V	3006 (3) Å
space group	A 2
d_c	1.12 g cm^{-3}
Z	4
$F(000)$	1084
λ(Cu-Kα)	1.5418 Å
μ(Cu-Kα)	1.2 mm^{-1}
Crystal dimensions	0.3 × 0.1 × 0.03 mm
$2\theta_{max}$	136°
Reflection $I > 2.5\sigma(I)$	2106
Refined parameters	320
R	0.10
R_w	0.11
S	0.4

It is interesting to note that the torsion angle C_2^β-C_2^α-C_2'-O_2 of only 15(1)° indicates a possible conjugation between the two double bonds and an increased delocalization extending from the backbone to the side chain atoms. An analogous conjugation between the α,β double bond and the nitrogen atom seems to be ruled out by the torsion angle C_1'-N_2-C_2^α-C_2^β of −113(1)°. The oxygen atom of the formyl group is *syn* planar to the C^α atom as already found in the crystal of other formyl peptides.[4] Among the peptide bonds the largest deviation from planarity is presented by that connecting the Δ^ZLeu with the Phe residue [ω_2 = 171.5(9)°] and might in part be a consequence of the conjugation between the carbonyl C_2'-O_2 and the α,β double bond. The torsion angle C_3''-O_3''-C_3'-O_3 of −1(1)° indicates that the carbonyl bond is *syn* planar to the ester bond as seen in general for esters.[15]

The Met side chain adopts a *t,t,g*$^-$ conformation: it can be noted that values of $\chi^3 \sim -60°$ less frequently occur with respect to the other staggered positions.[16] The torsion angles defining the Δ^ZLeu side chain are χ_2^1 = 11(1)°, $\chi_2^{2,1}$ = −105(1)°, $\chi_2^{2,2}$ = 137(1)°. This conformation greatly differs from that observed in the saturated Leu residues, and closely resembles the corresponding average weighted values of 0°, −110°, and 130° found

Table II Final Fractional Coordinates of 1 and B_{eq} (Å^2) with ESDs in Parentheses for the Nonhydrogen Atoms ($B_{eq} = \frac{4}{3}\Sigma_i\Sigma_j a_i a_j \beta_{ij}$)

	x	y	z	B_{eq}
O_0	0.638 (2)	0.0588 (8)	0.2709 (3)	6.9 (3)
C'_0	0.684	−0.0019 (9)	0.2510 (4)	5.2 (3)
N_1	0.728	−0.0029 (8)	0.2123 (4)	5.7 (3)
C_1^α	0.737 (2)	0.0728 (9)	0.1885 (4)	5.2 (3)
C_1^β	0.782 (2)	0.0529 (9)	0.1454 (5)	5.7 (4)
C_1^γ	0.808 (3)	0.130 (1)	0.1193 (5)	7.3 (5)
S_1^δ	0.852 (1)	0.109[a]	0.0660 (1)	10.0 (2)
C_1^ϵ	1.159 (5)	0.084 (2)	0.074 (1)	15 (1)
C'_1	0.509 (2)	0.1207 (8)	0.1894 (3)	4.0 (3)
O_1	0.319 (1)	0.0877 (7)	0.1811 (3)	5.8 (3)
N_2	0.536 (1)	0.2011 (7)	0.1999 (3)	3.6 (2)
C_2^α	0.335 (2)	0.2533 (7)	0.1986 (3)	3.5 (2)
C_2^β	0.291 (2)	0.3153 (8)	0.1730 (4)	4.2 (3)
C_2^γ	0.421 (4)	0.335 (1)	0.1356 (6)	8.6 (6)
$C_2^{\delta_1}$	0.586 (3)	0.412 (1)	0.1500 (7)	8.6 (6)
$C_2^{\delta_2}$	0.258 (4)	0.357 (1)	0.1007 (5)	9.3 (7)
C'_2	0.171 (2)	0.2421 (8)	0.2312 (3)	3.9 (3)
O_2	−0.020 (1)	0.2753 (7)	0.2299 (3)	4.7 (2)
N_3	0.250 (2)	0.1976 (8)	0.2634 (3)	4.5 (2)
C_3^α	0.119 (2)	0.1923 (9)	0.2993 (4)	4.8 (3)
C_3^β	0.254 (2)	0.1430 (9)	0.3333 (4)	5.2 (3)
C_3^γ	0.132 (2)	0.139 (8)	0.3717 (4)	4.9 (3)
$C_3^{\delta_1}$	−0.064 (3)	0.093 (1)	0.3735 (5)	7.1 (5)
$C_3^{\delta_2}$	0.210 (4)	0.187 (1)	0.4058 (5)	8.0 (6)
$C_3^{\epsilon_1}$	−0.180 (3)	0.087 (1)	0.4075 (5)	7.6 (5)
$C_3^{\epsilon_2}$	0.104 (5)	0.185 (1)	0.4407 (6)	10.3 (8)
C_3^ζ	−0.109 (3)	0.135 (1)	0.4406 (5)	7.6 (5)
C'_3	0.055 (2)	0.2756 (8)	0.3136 (4)	4.6 (3)
O_3	0.190 (1)	0.3307 (7)	0.3188 (3)	5.1 (2)
O''_3	0.166 (1)	0.2780 (7)	0.3232 (3)	5.8 (3)
C''_3	−0.230 (2)	0.352 (1)	0.3411 (8)	9.2 (7)
O_w[b]	0.399 (6)	0.350 (2)	0.5348 (8)	16 (1)
O'_w[b]	0.23 (2)	0.380 (6)	0.502 (3)	12 (2)
C_4	0.5000[a]	0.475 (4)	0.0000[a]	12 (1)
C_5	0.312 (5)	0.362 (4)	−0.0181 (6)	15 (1)
C_6	0.5000[a]	0.305 (2)	0.0000[a]	10 (1)
C_7	0.321 (6)	0.445 (3)	−0.017 (1)	16 (1)

[a] These positional parameters were kept fixed during the refinement.
[b] An occupancy factor of 0.8 and 0.2 were given to O_w and O'_w respectively during the refinement.

for Δ^ZLeu containing peptides.[8] The Phe side chain adopts an extended conformation with $\chi_3^1 = 177.2(8)°$, $\chi_3^{2,1} = 73(1)°$, and $\chi_3^{2,2} = -103(1)°$.

Crystal Packing

Two intermolecular hydrogen bonds characterize the packing: the former involves the NH and CO groups of Δ^ZLeu residues succeeding along the a direction; the latter, the Met NH and Phe CO groups of screw-related molecules along b. Their relevant geometric parameters are reported in Table IV together with those of the intramolecular hydrogen bond. It can be noted that in all cases the H···A contact is smaller than their van der Waals radii sum.

A view of the crystal packing is shown in Figure

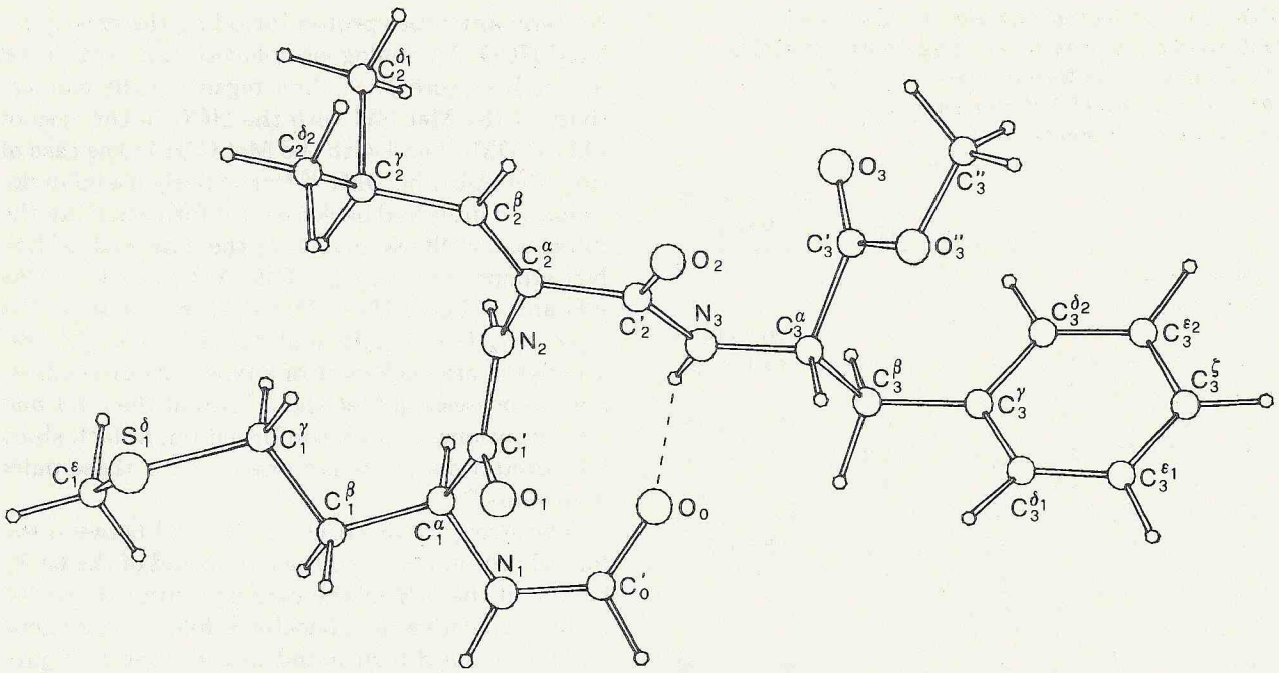

Figure 2. A perspective view of the peptide 1 crystal conformation.

3. Layers of intermolecular hydrogen-bonded peptides extend along the *a* and *b* directions. Adjacent layers related by the twofold axis extend along *c* and give rise, because of their wavy shape, to adjacent empty spaces, channels, running along *a*, which occlude alternatively benzene or water molecules. The outer surfaces of the peptide layers, which are the internal surfaces of the channels, are hydrophobic, so that the guest molecules are all surrounded by nonpolar groups.

Two carbon atoms of the benzene molecule lie on the twofold axis running along *b*. In the channel each benzene ring is sandwiched between the methyl groups of two Δ^ZLeu residues belonging to opposite layers: the shortest interatomic contact among these groups is $C_6 \cdots C_3^{\delta 2}$ of 3.81(3) Å. The twofold axis symmetry-related Phe rings, on one side, and the Met sulfur atoms, on the other side, are the other boundary groups of the channel. The shortest interatomic contacts that the benzene molecule forms with these groups are $C_4 \cdots C_3^{\zeta}$ at $-x, \frac{1}{2}+y, \frac{1}{2}-z$ of 4.06(3) Å and $C_6 \cdots S_1^{\delta}$ of 4.21(2) Å. In the channel, adjacent benzene molecules are at van der Waals distances: the shortest contact between carbon atoms is 3.87(3) Å, occurring between the C_5 atoms of two adjacent rings.

The twofold axis symmetry-related Phe rings and Met sulfur atoms belonging to facing layers are also the boundary groups of the adjacent channels where the water molecules are occluded, but at variance the methyl ester groups surround the guest molecules in the middle part of this channel. The water oxygen is spread out in this hydrophobic region and it was possible to assign at least two main positions, referred to as O_W and O'_W, having occupancy factor 0.80 and 0.20, respectively. The shortest interatomic contacts between the water oxygen and the channel atoms are $O_W \cdots C_3^{\delta 2}$ at $1-x, y, 1-z$ of 3.84(3) Å and $O'_W \cdots C_3^{\varepsilon 2}$ of 3.78(3) Å. Couples of twofold symmetry-related water molecules form hydrogen bonds: the $O_W \cdots O_W$ and $O'_W \cdots O'_W$ distances are 2.67(2) and 2.58(3) Å, respectively.

^{1}H-NMR Studies

The nmr spectrum of HCO-Met-Δ^ZLeu-Phe-OMe (1) in $CDCl_3$ is shown in Figure 4. The HCO singlet is easily recognized by its characteristic chemical shift (δ = 8.09 ppm). The assignment of the three NH groups is unequivocal: the Δ^ZLeu NH signal appears as a singlet; the Met and Phe NH doublets have been identified by spin decoupling experiments.

In order to gain information on the preferred solution conformation, nuclear Overhauser effect (NOE) experiments have been performed; part of the rotating frame NOE spectroscopy (ROESY) spectrum is shown in Figure 5. The estimates of the cross peaks relative intensities are reported, on an arbitrary scale, in Table V. A preliminary observation concerns the absence of NOEs between Met

Table III Selected Torsion Angles (°) of 1 Obtained by X-Ray Crystallographic Analysis (ESDs are in the Range 0.8–1.7°) and by MD Simulation (RMS Fluctuations are Given in Parentheses)

		Crystal	MD Average Value
Peptide backbone			
$O_0—C'_0—N_1—C^{\alpha}_1$		3	
$C'_0—N_1—C^{\alpha}_1—C'_1$	ϕ_1	−55	−79.2 (14.8)
$N_1—C^{\alpha}_1—C'_1—N_2$	ψ_1	129.7	93.1 (12.8)
$C^{\alpha}_1—C'_1—N_2—C^{\alpha}_2$	ω_1	175.0	
$C'_1—N_2—C^{\alpha}_2—C'_2$	ϕ_2	72.2	72.9 (13.1)
$N_2—C^{\alpha}_2—C'_2—N_3$	ψ_2	14.3	−9.5 (11.7)
$C^{\alpha}_2—C'_2—N_3—C^{\alpha}_3$	ω_2	171.5	
$C'_2—N_3—C^{\alpha}_3—C'_3$	ϕ_3	−50.4	−128.3 (27.8)
$N_3—C^{\alpha}_3—C'_3—O''_3$	ψ^{T}_3	137.2	133.1 (25.7)
$C^{\alpha}_3—C'_3—O''_3—C''_3$	ω_T	173.5	
$C''_3—O''_3—C'_3—O_3$	θ	−1	
Met side chain			
$N_1—C^{\alpha}_1—C^{\beta}_1—C^{\gamma}_1$	χ^1_1	−176.6	−160.0 (13.6)
$C'_1—C^{\alpha}_1—C^{\beta}_1—C^{\gamma}_1$	χ'_1	61.3	
$C^{\alpha}_1—C^{\beta}_1—C^{\gamma}_1—S^{\delta}_1$	χ^2_1	−177.7	−90.9 (42.4)
$C^{\beta}_1—C^{\gamma}_1—S^{\delta}_1—C^{\epsilon}_1$	χ^3_1	−79	−171.0 (49.6)
Δ^z leu side chain			
$N_2—C^{\alpha}_2—C^{\beta}_2—C^{\gamma}_2$	χ^1_2	11	0.2 (8.9)
$C'_2—C^{\alpha}_2—C^{\beta}_2—C^{\gamma}_2$	χ'_2	−175	
$C^{\alpha}_2—C^{\beta}_2—C^{\gamma}_2—C^{\delta_1}_2$	χ^{21}_2	−105	−122.0 (42.8)
$C^{\alpha}_2—C^{\beta}_2—C^{\gamma}_2—C^{\delta_2}_2$	χ^{22}_2	137	
Phe side chain			
$N_3—C^{\alpha}_3—C^{\beta}_3—C^{\gamma}_3$	χ^1_3	177.2	−117.6 (50.9)
$C'_3—C^{\alpha}_3—C^{\beta}_3—C^{\gamma}_3$	χ'_3	52.2	
$C^{\alpha}_3—C^{\beta}_3—C^{\gamma}_3—C^{\delta_1}_3$	χ^{21}_3	73	92.6 (24.2)
$C^{\alpha}_3—C^{\beta}_3—C^{\gamma}_3—C^{\delta_2}_3$	χ^{22}_3	−103	

NH and any other proton including the closely related HCO. An analogous behavior can be deduced by the literature NOE data regarding the connectivity of the Met NH with the HCO in the case of f MLP-OMe[17] and with the Met $C^{\alpha}H$ in the case of Boc-Met-Aib-Phe-OMe.[18] Particularly useful in defining the preferred backbone conformation are the interresidue NOEs involving the Phe and Δ^ZLeu NH groups. The strong NOEs Δ^ZLeu NH···Phe NH and Δ^ZLeu NH···Met $C^{\alpha}H$, which are of the type $N_{i+2}H···N_{i+3}H$ and $C^{\alpha}_{i+1}H···N_{i+2}H$, respectively, are diagnostic of a type II β-turn conformation possessing Met and Δ^ZLeu at the $i+1$ and $i+2$ positions. In such conformation, in fact, short interproton distances are expected for these pairs of protons.[19,20]

The strong NOE HCO···Phe NH between the formyl proton bound to the amino end of the backbone and the NH of the carboxy-terminal residue is also indicative of a backbone folding analogous to that of the β-turn found in the crystal (Figure 2). This latter conformation, however, possesses an hydrogen bond that maintains the formyl proton on the opposite side of the Phe NH—the corresponding interproton distance being 4.04 Å, a value not compatible with the strong NOE observed in solution. This nmr effect, however, can be still consistent with a type II β-bend, if the small size of the formylic group is taken into account. As a consequence of this feature, both the carbonyl oxygen and its proton are in spatial proximity with the Phe NH; thus, dynamic fluctuation of the β-bend structure can determine short HCO···Phe NH interproton distances. The nonlinearity between interproton dis-

Table IV Hydrogen-Bond Data of Compound 1 in the Crystal and Obtained by MD Simulation (For the Crystal Data ESDs are in the Range 0.02–0.03 Å for the Contacts and 0.7°–1.5° for the Angles, Respectively)

Donor (D)	Acceptor (A)	H···A (Å)	D···A (Å)	D—H···A (°)	C=O···H (°)	Occurrence (% Time)
			"Crystal" [a]			
N_1	O^{a}_3	1.96	2.95	170	142	
N_2	O^{b}_2	1.87	2.87	172	123	
N_3	O_0	2.21	3.15	155	139	
			"MD"			
N_3	O_0		3.1	161		13
N_3	O_1		2.9	146		38
N_2	O_0		3.0	143		14

[a] Symmetry code: (*a*) $-x+1, y-1/2, -z+1/2$; (*b*) $x+1, y, z$.

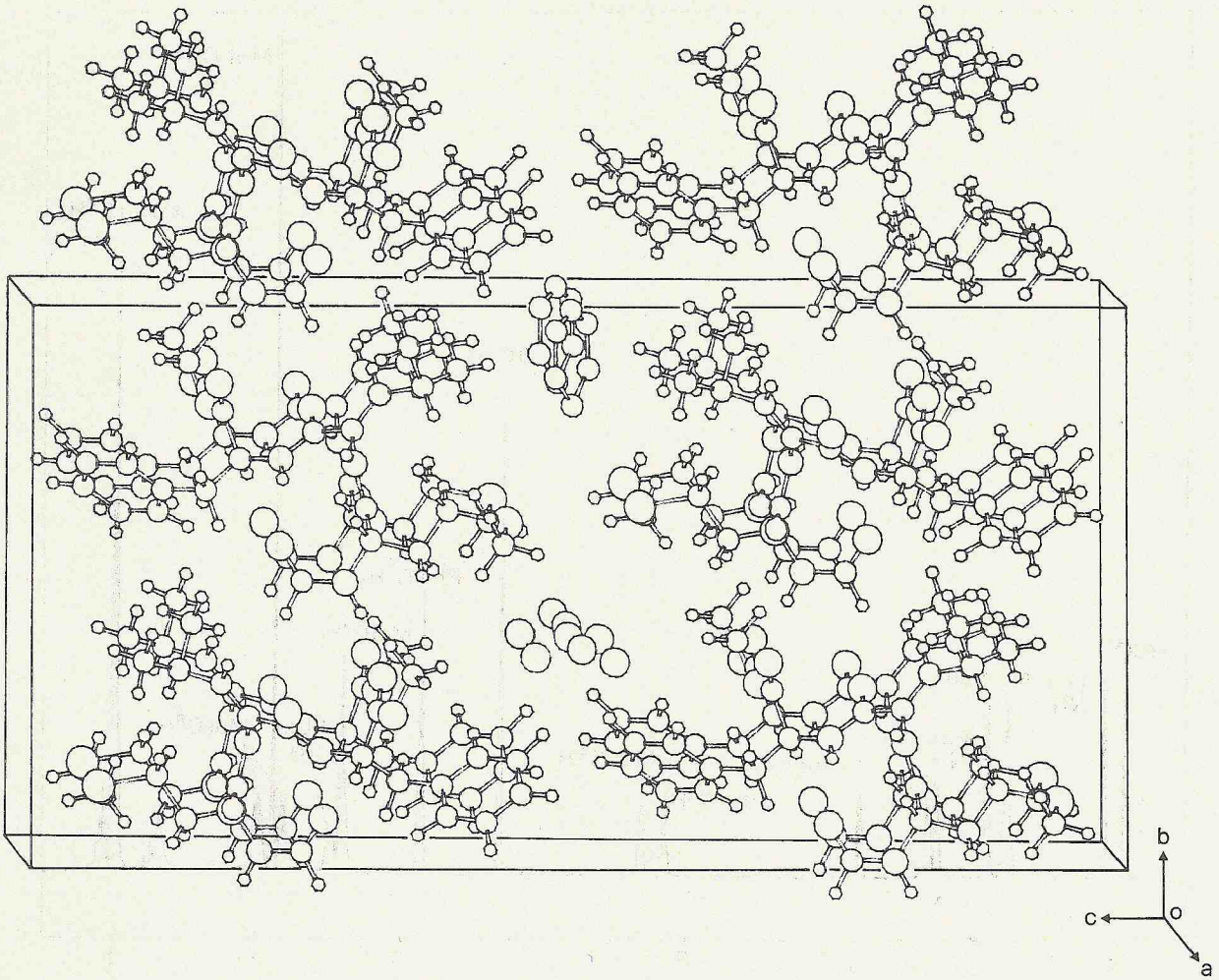

Figure 3. A view of the crystal packing showing the channels where benzene and water molecules are occluded. Both positions for the water molecule have been reported. The hydrogen atoms of the molecules are not drawn.

tance and NOE effect, which overweighs short distances, can account for the strength of this signal.

The last strong interresidue NOE Δ^ZLeu $C^\beta H \cdots$ Phe NH is not consistent with a type II β-bend.[19,21] This latter conformation, found in the crystal, exhibits in fact an interproton distance of 4.3 Å and a small value of ψ_2 (14°). Interproton distances compatible with the observed NOE are expected only for extended or semiextended conformations with corresponding ψ values in the range of ±100 to ±180°.[21] Thus, the observation of the above nmr effect is indicative of a certain population of extended conformers. The $J_{NH\text{-}C^\alpha H}$ values (7.3–7.7 Hz) observed for Met and Phe residues, corresponding to φ values of $\sim -90°$ and $-150°$,[22] are also in accordance with a conformational averaging between folded and extended conformers.

The chemical shift of the NH protons are practically concentration independent in $CDCl_3$ solution over the range 10^{-4}–10^{-1} M (data not shown), thus indicating that aggregation occurs, if any, at very limited extent. The involvement of NH protons in intramolecular hydrogen bonding was evaluated on the basis of change in chemical shift experienced upon addition of DMSO-d_6 to a $CDCl_3$ solution. As shown in Figure 6, the Met and Δ^ZLeu resonances move downfield with increasing concentration of $(CD_3)_2SO$, while the Phe NH group is less affected by the change of the solvent composition. The reduced solvent perturbation observed for Phe NH is consistent with its involvement in an intramolecular hydrogen bond, suggestive of a significant population of β-turn conformers.

Molecular Dynamics

The torsion angles obtained by the molecular dynamics (MD) simulation and their root mean square

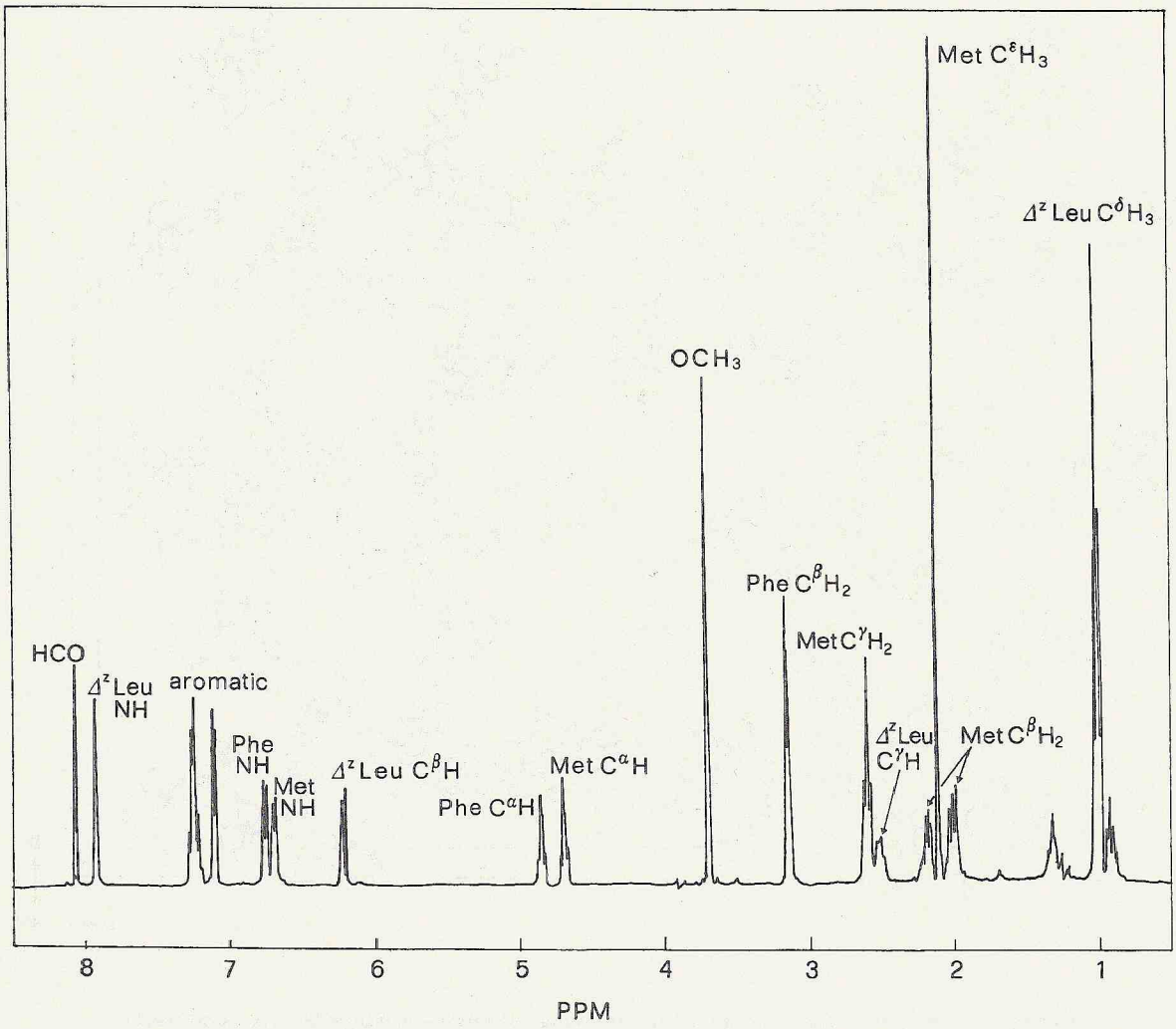

Figure 4. ^{1}H-nmr spectrum of the peptide **1** in $CDCl_3$ solution (5 m*M*).

fluctuations (rms) are reported in Table III together with the values found in the crystal conformation. A comparison of the two sets of data shows that the type II β-turn conformation found in the crystal is retained in the MD simulation with small flexibility of the backbone: the largest difference is that regarding the ψ of the Met residue. Larger flexibility seems to affect the terminal part of the backbone as shown by the values of the rms fluctuations of the Phe residue. Even larger fluctuations affect the side-chain torsion angles. Only the χ^1 of Met and Δ^ZLeu residues do not show this behavior; in both cases a bond making part of the β-turn structure is involved (N_1-C_1^{α} and N_2-C_2^{α}, respectively); furthermore, the rotation about the C_2^{α}-C_2^{β} bond is prevented by the unsaturation. The limited fluctuation of the Phe χ^2 is a consequence of the restrictions imposed by the interactions between the aromatic ring and the adjacent backbone atoms; this results in the well-known rotameric preference for χ^2 values of 90 $\pm$ 20°.[23]

Interproton Distances

The NOEs together with the interproton distances obtained from the crystal conformation and MD simulation are reported in Table V. An examination of these data reveals a good agreement among nmr, x-ray, and MD results except for HCO-Phe NH and Phe NH-Δ^ZLeu $C^{\beta}H$ interproton distances. In order to clarify this point, the fluctuation of these distances during the MD simulation has been determined and reported in Figure 7. It can be observed that whereas the distance involving the Phe and Δ^ZLeu residues remains practically constant, the HCO-Phe NH distance undergoes large fluctuations,

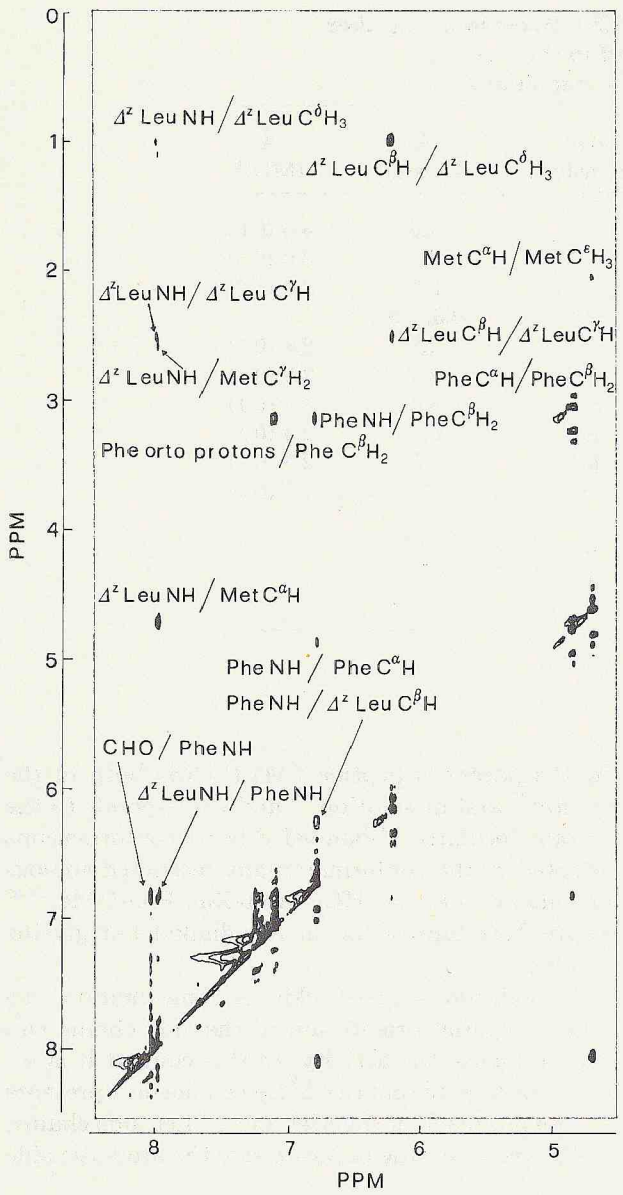

Figure 5. Dipolar correlated ROESY spectrum of the peptide **1**. Only the region from 8.5 to 5.5 ppm is reported.

in the range 2.8–6.0 Å. Furthermore, by allowing small variations to the appropriate φ and ψ torsion angles, short HCO-Phe NH interproton distances can be produced with maintenance of the β-turn structure (data not shown). Thus, as already discussed in the nmr section, the nonlinearity of NOE with the distance together with the possibility of dynamic fluctuation can account for the disagreement between nmr, x-ray, and MD results, concerning the HCO-Phe NH distance. Figure 7 clearly shows, however, that the Phe NH-Δ^ZLeu C$^\beta$H interproton distance does not fluctuate and this finding is in accordance with the partial double-bond character of the involved bonds. In this case short interproton distances, compatible with the strong NOE observed, can be only obtained if an open conformation of the backbone is considered. It should be pointed out that even a low percentage of this conformation in solution can account for the observed NOE.

Hydrogen Bonds

The occurrence of hydrogen bonds during the MD simulation has been analyzed. The results, reported in Table IV, show that three different bonds are present in the simulation. The Phe NH···HCO coincides with that found in the type II β-bend crystal conformation. However, the presence of the other two bonds is typical of seven-membered γ-turn conformations.

Biological Activity

The biological activity of **1** has been determined on human polymorphonuclear leukocytes (PMNs) and compared to that of the parent tripeptide fMLP-OMe. The directed migration (chemotaxis), superoxide anion production, and lysozyme release have been measured.

As shown in Figure 8, the unsaturated analogue **1** is practically inactive as chemoattractant at all the tested concentrations (10^{-11}–$10^{-5}M$). In contrast, analogue **1** exhibits an activity significantly higher ($p < 0.01$) than the parent tripeptide in the superoxide anion production, and stimulates the enzyme release in the same way as fMLP-OMe ($p = 0.05$).

Conclusions

Several conformationally restricted analogues of fMLP have been synthesized for their potential biological activities, and more specifically, for a better understanding of the nature of the bioactive (receptor-bound) conformation. The conformational flexibility of the native fMLP,[24] evidenced by several studies based on x-ray diffraction, nmr spectroscopy, and potential energy calculations, can be considered, in fact, the feature responsible for the lack of selectivity shown by this ligand, which can stimulate a series of neutrophil functions ranging from chemotaxis to superoxide anion release.

Our results show that the replacement of the central Leu of fMLP-OMe with the corresponding α,β-unsaturated residue induces a type-II β-bend con-

Table V Observed NOEs in the ROESY Spectrum Together with Interproton Distances (Å) Found in the Crystal and Obtained by MD Simulation for Compound 1

	NOE Intensity[a]	Å (Crystal)	Å (MD)[b]
HCO · · · Phe NH	s	4.0	4.0 (0.6)
Δ^zLeu NH · · · Phe NH	s	2.7	3.0 (0.3)
Δ^zLeu NH · · · Met CH^{α}	s	2.1	2.2 (0.2)
Phe CH^{β} · · · Aromatic ortho CH	s	2.3, 2.5	
Δ^zLeu CH^{β} · · · Δ^zLeu CH^{δ}	s	2.5	2.8 (0.1)
Phe CH^{α} · · · Phe CH^{β}	s	2.4	2.5 (0.1)
Phe NH · · · Δ^zLeu CH^{β}	s	4.3	4.2 (0.1)
Phe NH · · · Phe CH^{β}	m	2.5	2.9 (0.3)
Δ^zLeu CH^{β} · · · Δ^zLeu CH^{γ}	m	3.2	2.9 (0.1)
Δ^zLeu NH · · · Δ^zLeu CH^{γ}	m	2.9	2.8 (0.4)
Δ^zLeu NH · · · Met CH^{γ}	w		
Δ^zLeu NH · · · Δ^zLeu CH^{δ}	w		
Met CH^{α} · · · Met CH_3	w		
Phe NH · · · Phe CH^{α}	w		

[a] s: Strong; m: medium; w: weak.
[b] RMS fluctuations are given in parentheses.

formation in which the new amino acid occupies the $(i + 2)$ position of the ten-membered pseudo cyclic system. This folded conformation has been found in the crystal and also represents the preferred conformation in $CDCl_3$ solution and in the MD simulation. This conformation differs from that adopted by the parent tripeptide fMLP-OMe both in the crystal[25] and in solution,[26] and corresponds to the intramolecularly H-bonded β-bend conformations adopted by the conformationally restricted analogs of general formula HCO-Met-Xaa-Phe-OMe,[27-29] where Xaa represents an α,α-dialkylated glycine residue.

In addition to the backbone conformation, the relative spatial orientation of the side chains will also influence the activity. In this context it is interesting to note that the Δ^zLeu analogue **1** presents a close approach of the Met and Δ^zLeu side chains, which leaves on the opposite side the aromatic side

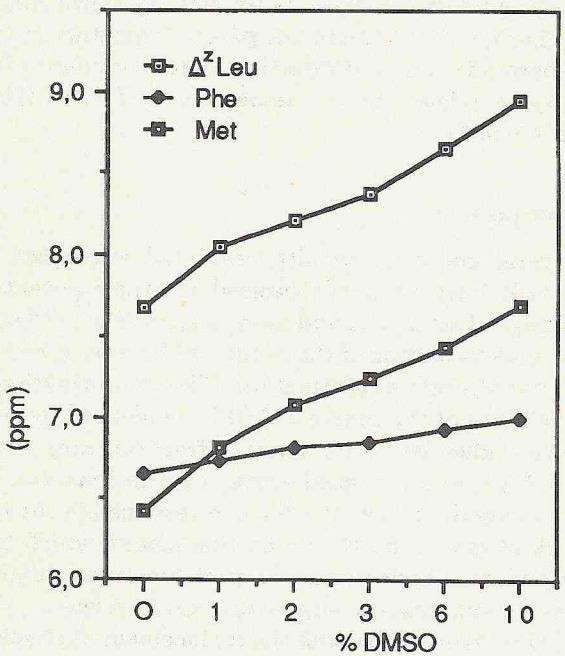

Figure 6. Chemical shift dependence of the NH resonances as a function of the DMSO-d_6 concentration (% v/v) in $CDCl_3$ solution.

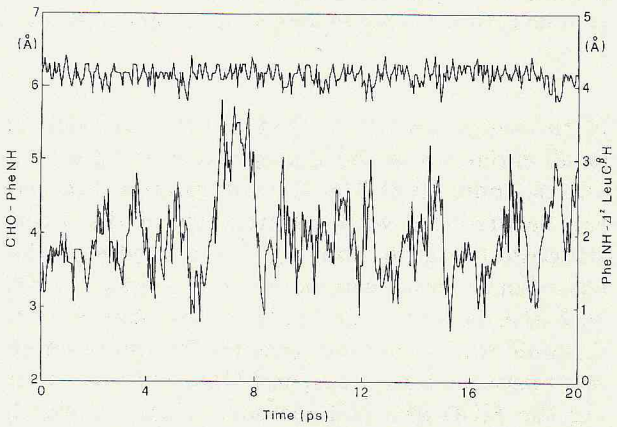

Figure 7. Fluctuations of the interproton distances: HCO · · · PheNH (lower trace, left ordinate) and PheNH · · · Δ^zLeuC$^{\beta}$H (upper trace, right ordinate).

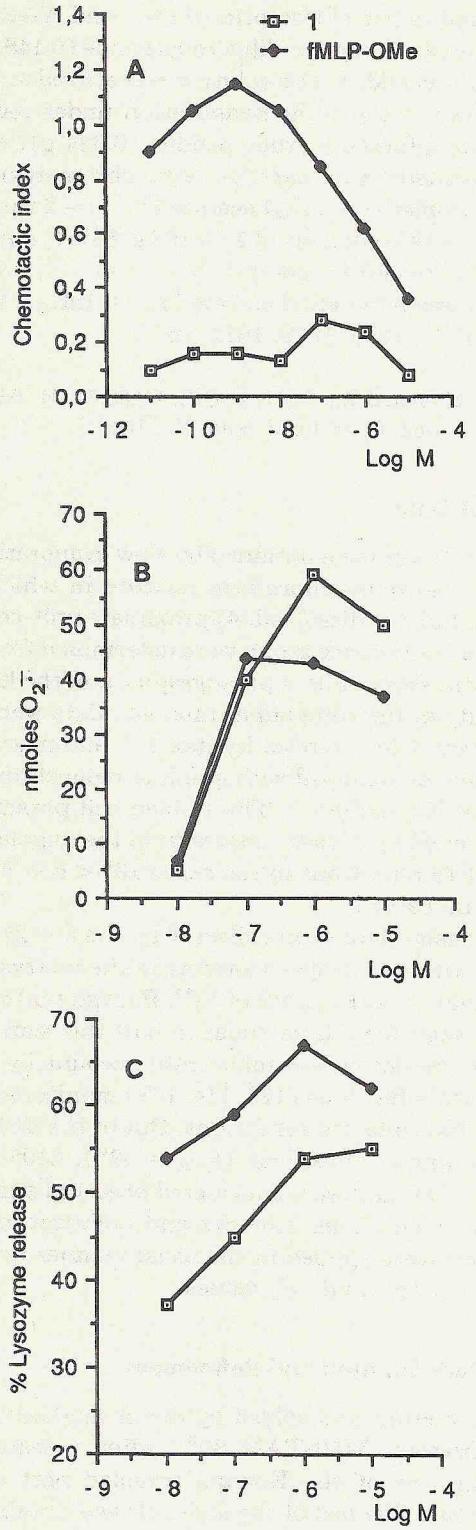

Figure 8. Biological activities of fMLP-OMe and its [Δ^ZLeu^2] analogue **1** toward human neutrophils. (A) Chemotactic activity. The points are mean of six separate experiments done in duplicate. Standard errors are in the 0.02–0.09 chemotactic index range. (B) Superoxide anion production. The points are mean of six separate experiments done in duplicate. Standard errors are in 0.1–4% range. (C) Release of neutrophil granule enzymes evaluated by determining lysozyme activity. The points are mean of five separate experiments done in duplicate. Standard errors are in 1–6% range.

chain of the C-terminal residue. This spatial arrangement differs from that found when the native ligand fMLP is cocrystallized with a formyl peptide receptor protein.[30] In this case the Met and the Phe side chains face each other, leaving the Leu side chain on the opposite side; this latter side chain orientation has been previously evidenced by us in the case of the conformationally constrained analogue [Thp^1, Ain^3]-fMLP-OMe (Thp: 4-aminotetrahydrothiopyran-4-carboxylic acid; Ain: 2-aminoindane-2-carboxylic acid), which adopts in the crystal an irregular folded conformation analogous to that of fMLP-OMe.[4]

The biological activity of **1** has been determined on human neutrophils; the results, reported in Figure 8, show that the Δ^ZLeu analogue is practically inactive as chemoattractant, but active in the superoxide anion production and granule enzyme release. Thus, the here described β-bend structure, adopted by the Δ^ZLeu analogue **1**, should allow an highly favorable interaction with the human formyl peptide receptor responsible for superoxide anion production and the lysozyme release. This selective behavior is opposite to that of the above-cited [Thp^1, Ain^3]fMLP-OMe analogue that, whereas highly active as chemoattractant, is practically inactive in the superoxide anion production.

Recently two variants[31] of the human formyl peptide receptor have been characterized and isolated. However, several aspects concerning the receptor functional heterogeneity and the control mechanism of the various biological responses are only just emerging in the literature.[32] Thus, the design and the study of ligands able to discriminate the receptor variants and the different biological responses seem an useful approach.[4,33] In this context, the here described conformationally constrained Δ^ZLeu analogue may represent a useful contribution for the development of selective ligands and for a better understanding of structure activity relationships.

EXPERIMENTAL

Peptide Synthesis

Melting points were determined with a Kofler hot stage apparatus and are uncorrected. Optical rotations were taken at 20°C with a Schmidt-Haensch

Polartronic D polarimeter in a 1 dm cell (c 1.0, $CHCl_3$). Infrared spectra (KBr disks) were recorded with a Perkin-Elmer 983 spectrophotometer. ^{1}H-nmr spectra were measured with a Varian XL-300 spectrometer in $CDCl_3$ (tetramethylsilane as internal standard). Column chromatographies were carried out using Merck silica gel 60 (230–400 mesh; 1:30). Thin layer and preparative layer chromatographies were performed on silica gel Merck 60 F_{254} plates. The drying agent was sodium sulfate.

Boc-Met-Δ^ZLeu-Phe-OMe. To a solution of Boc-Met-OH (0.634 g, 2.54 mmol) in dry tetrahydrofuran (4.2 mL) *N,N'*-dicyclohexylcarbodiimide (0.525 g, 2.54 mmol) was added at −10°C, and after stirring for 20 min, Δ^ZLeu · NCA[7] (0.329 g, 2.12 mmol) and dry pyridine (0.17 mL, 2.12 mmol) were added. Stirring was continued at −10°C for 2 h and then at room temperature overnight. To the reaction mixture Phe-OMe · HCl (0.64 g, 2.97 mmol), dry tetrahydrofuran (4.2 mL), triethylamine (0.42 mL, 2.97 mmol), and *N*-methylmorpholine (0.33 mL, 2.97 mmol) were added. After stirring for 2 h, the solvent was removed under reduced pressure. The residue was dissolved in chilled ethyl acetate and *N,N'*-dicyclohexylurea was filtered off. The filtrate was similarly worked up to give an oil (1.49 g), which was chromatographed on a silica gel column eluting with dichloromethane and dichloromethane-ether (9 : 1). The nearly homogeneous product (0.614 g) was further purified by preparative layer chromatography [dichloromethane-ethyl acetate (7 : 3)] to give pure title tripeptide (0.51 g, 46%), mp 118°C (from ethyl acetate). $[a]_D$ + 18°. R_f: 0.51 in dichloromethane-ethyl acetate (7 : 3). Infrared ν_{max}: 3376, 3344, 1748, 1622 cm^{-1}. ^{1}H-nmr, δ 1.00 [6H, apparent t, $(CH_3)_2$-CH], 1.45 [9H, s, $C(CH_3)_3$], 1.96 and 2.14 (2H, two m, Met β-CH_2), 2.09 (3H, s, S-CH_3), 2.52 (1H, m, Δ^ZLeu γ-CH), 2.60 (2H, t, J = 7.5 Hz, CH_2-S), 3.14 (2H, d, J = 6 Hz, Phe β-CH_2), 3.69 (3H, s, O-CH_3), 4.29 (1H, apparent q, Met α-CH), 4.86 (1H, apparent q, Phe α-CH), 5.29 (1H, br d, NH-COO), 6.28 (1H, d, J = 10 Hz, Δ^ZLeu β-CH), 6.76 (1H, poorly resolved d, Phe NH), 7.09–7.32 (5H, m, aromatic), 7.68 (1H, s, Δ^ZLeu NH).

Anal. Calculated for $C_{26}H_{39}N_3O_6S$: C, 59.86; H, 7.54; N, 8.05%. Found: C, 59.93; H, 7.84; N, 7.78%.

HCO-Met-Δ^ZLeu-Phe-OMe (1). Boc-Met-Δ^ZLeu-Phe-OMe (0.261 g, 0.5 mmol) was dissolved in 98% formic acid (2 mL) and the mixture was stirred at room temperature for 18 h. After removal of the excess of formic acid under vacuum, the residue was dissolved in dry chloroform (2 mL) and *N*-ethoxycarbonyl-2-ethoxy-1,2-dihydroquinoline (0.148 g, 0.6 mmol) was added. The solution was stirred at room temperature for 18 h. Evaporation under reduced pressure afforded a crude residue (0.324 g), which was purified on preparative layer chromatography [dichloromethane-ethyl acetate (1 : 1)—2 runs] to give pure title compound 1 (0.198 g, 88%), mp 151–152°C (from ethyl acetate). $[a]_D$ + 17°. R_f: 0.24 in dichloromethane-ethyl acetate (1 : 1). Infrared ν_{max}: 3341, 1726, 1696, 1679, 1614 cm^{-1}.

Anal. Calculated for $C_{22}H_{31}N_3O_5S$: C, 58.77; H, 6.95; N, 9.35%. Found: C, 58.40; H, 6.85; N, 9.05%.

Crystal Data

Crystals have been obtained by slow evaporation of a 1 : 1 benzene–chloroform mixture in which the compound was dissolved. Approximate unit-cell parameters and space group were determined from oscillation, Weissenberg photographs, and the known chirality of the compound. Intensity data were collected on a four circles Syntex $P2_1$ automatic diffractometer equipped with graphite monochromator and Cu-Kα radiation. The refined cell parameters determined by a least-squares fit of the angular setting of 18 reflections in the range $10° < \theta < 30°$ are given in Table I.

Intensity data were collected by the $\theta - 2\theta$ technique with a scan speed varying in the interval 1.5–14.5° min^{-1} over a range of 1.6°. Background counts were taken for a time equal to half the scan time. The x-ray decay was taken into account by three standard reflections ($12\bar{3}$, $11\bar{4}$, 101) monitored after every 100 collected reflections. Out of the 3103 collected unique reflections (θ_{max} = 68°), 2106 had $I > 2.5\,\sigma(I)$, and were considered observed and used in the calculations. Lorentz and polarization corrections were applied in the usual manner in order to obtain $|E|$ and $|F|$ values.

Structure Solution and Refinement

The structure was solved by direct methods using the program MULTAN 80[34]; after repeated attempts, one of the E-maps revealed part of the backbone. The rest of the molecule was obtained by Fourier recycling. The four carbon atoms of the benzene molecule belonging to the asymmetric unit were recognized in the Fourier difference map, where two additional peaks, having about 4 : 1 electron density ratio, were interpreted as due to a disordered oxygen of a water molecule. This interpretation was

also supported by the ^{1}H-nmr spectra of the crystals dissolved in $CDCl_3$, from which a 1 : 1 : 0.5 stoichiometric ratio was obtained for the peptide, water, and benzene molecules, respectively. The two positions of the water oxygen were refined isotropically with occupancy factors 0.8 and 0.2, and referred to as O_W and O'_W, respectively. All the other nonhydrogen atoms were refined anisotropically by full-matrix least-squares method. The function $\Sigma w(|F_0| - |F_c|)^2$ was minimized where $w = (a + |F_0| + c|F_0|^2)^{-1}$ with a and c equal to 2 $F_{0(min)}$ and $2/F_{0(max)}$, respectively. After each cycle of refinement, the H atoms were generated at the expected positions with C-H and N-H bond length, respectively, of 1.09 and 1.00 Å, and thermal isotropic parameters deduced from the carrier atoms. Scattering factors were taken from Ref. 35. The final fractional coordinates together with B_{eq} of the nonhydrogen atoms are given in Table II. All the calculations were performed on the D.G. ECLIPSE MV/8000 II using the package of programmes of Ref. 36.

Two-Dimensional NMR Spectroscopy

Spectra were run on a Bruker AM 400 instrument operating at 400.13 MHz at 30°C. Homonuclear two-dimensional (2D) nmr experiments were performed in the phase sensitive mode using time proportional phase incrementation phase cycle[37,38] using 2K of memory typically for 512 increments. Spectral width and the number of scans were optimized to obtain best resolution and a satisfactory signal to noise ratio.

Correlation experiments were performed in the double quantum filtered mode.[39] NOE dipolar correlated 2D spectra were obtained by using ROESY.[40,41] The mixing time for the magnetization exchange applied was 200 ms. Data were weighted by a sine-bell apodization function shifted typically of T/3 in both dimensions and processed on a micro Vax II with the 2D-nmr software written in FORTRAN 77. The program was kindly provided by Prof. R. Kaptein, Department of Organic Chemistry, Afd. NMR, Utrecht, The Netherlands. A matrix of 1024 × 1024 phase sensitive absorption spectra was thus obtained with a digital resolution of 5.4 Hz point. An accurate baseline correction was carried out in both dimensions by using a polynomial fit provided by the same program.

Restrained MD

Restrained MD calculations in vacuo were performed with programs from the Groningen molecular simulations system (GROMOS) software package.[42–44] The applied empirical potential energy function contains terms representing covalent bond stretching, bond angle bending, harmonic dihedral angle bending (out-of-plane, out-of-tetrahedral configuration), sinusoidal dihedral torsion, van der Waals, and electrostatic interactions.[44] The parameters for the bonded and nonbonded interactions functions used in the simulation were the ones included in the GROMOS package, except for the sinusoidal dihedral torsion around the C^{α}_2-C'_2 bond that has partial double-bond character. An energy barrier of 23.0 kJ · mol^{-1} for this torsion angle was chosen. A dielectric permittivity $\epsilon = 1$ was used and the cutoff radius for the nonbonded interactions was chosen in order to include all interactions. In addition, an attractive half-harmonic restraining potential was applied to force the molecule to satisfy selected NOE distances[43]:

$$V_{DR}(d_{kl}) = \tfrac{1}{2} k_{DR}(d_{kl} - d^*_{kl})^2 \quad \text{if } d_{kl} \geq d^*_{kl}$$

$$V_{DR}(d_{kl}) = 0 \quad \text{if } d_{kl} \leq d^*_{kl}$$

where k_{DR} was 40 kJ · mol^{-1} Å^{-2}. In order to translate the NOE information into distances, ranges d^*_{kl} 3, 4, and 5 Å were chosen for strong, medium, and weak NOEs, respectively.[45] For the evaluation of this potential, all protons were treated explicitly. For all other terms, only protons attached to nitrogen or oxygen atoms were treated explicitly. For other protons, a united atom approach was chosen.

The bond stretching term was not included in the calculation; the SHAKE[46] algorithm was used to constrain bond lengths. The initial conformation of the MD simulation was the one obtained by the crystal structure analysis. All atoms were given an initial velocity obtained from a Maxwellian distribution at T = 300 K. The constancy of the temperature during the run was obtained by a coupling with an external bath[47] with a time constant of 0.1 ps. A time step of 0.002 ps was used for the simulation.

A first 20-ps simulation was performed by including all the restraining potentials that account for the experimental NOEs (run I). It was followed by a second 20-ps simulation, starting from the same conformation, in which the restraining potentials on those protons whose distances did not satisfy the NOE were left out (run II).

The results of the two simulations do not significantly differ from each other and the data of the second 20-ps MD simulation (run II), including all the restraining potentials that account for the experimental NOEs, except for those between protons

HCO · · · Phe NH and Phe NH · · · Δ^ZLeu C$^\beta$H, are reported. No large fluctuations in the potential energy have been observed so that all the conformations explored during the simulations are energetically permitted.

Biological Assay

Cells. Human PMNs were purified employing the standard techniques of dextran (Pharmacia) sedimentation, centrifugation on lymphocyte separation medium (Flow S.p.A.), and hypotonic lysis of red cells. The cells were washed twice and resuspended in KRPG (Krebs-Ringer-phosphate containing 0.1% w/v glucose, pH 7.4) at a concentration of 50 $\times 10^6$ cells/mL. The percentage of neutrophils was 98–100% pure.

Random Locomotion. Random locomotion was performed with a 48-well microchemotaxis chamber (Bio Probe, Italy) and the migration into the filter was evaluated by the method of leading-front.[48]

Chemotaxis. In order to study the potential chemotactic activity, each peptide was added to the lower compartment of the chemotaxis chamber. Peptides were diluted from a stock solution ($10^{-2}M$ in dimethylsulfoxide) with KRPG containing 1 mg/mL of bovine serum albumin (Orha Beringwerke, BRD) and used at concentrations ranging from 10^{-11} to $10^{-5}M$. Data were expressed in term of chemotactic index, which is the ratio of (migration toward test attractant minus migration toward the buffer)/migration toward the buffer.

Superoxide Anion (O_2^-) Production. O_2^- release was monitored continuously in a thermostated spectrophotometer as superoxide dismutase-inhibitable reduction of ferricytochrome c (Sigma, USA), as described elsewhere.[49] At zero time, different amounts (10^{-8}–$10^{-5}M$) of each peptide were added and absorbance change accompanying cytochrome c reduction was monitored at 550 nm. Results were expressed as net nmoles of $O_2^-/2 \times 10^6$ PMNs/5 min. Neutrophils were incubated with 5 μg/mL cytochalasin B (Sigma) for 5 min prior to activation by peptides.

Enzyme Assay. Release of neutrophil granule enzymes was evaluated by determining lysozyme activity[49]; this was quantified nephelometrically by the rate of lysis of cell wall suspension of *Micrococcus lysodeikticus* (Sigma). Enzyme release was expressed as a net percentage of total enzyme content released by 0.1% Triton X-100. Total enzyme activity was 85 ± 1 μg/1 $\times 10^7$ PMNs/min. To study the degranulation-inducing activity of each peptide, PMNs were first incubated with cytochalasin B for 15 min at 37°C and then in the presence of each peptide in a final concentration of 10^{-8}–$10^{-5}M$ for a further 5 min.

Statistical Analysis. The nonparametric Wilcoxon test was used in the statistical evaluation of differences between groups.

REFERENCES

1. Harvath, L. (1991) *Experientia,* **59** (Suppl. Cell Motil. Factors), 35–52.
2. Freer, R. J., Day, A. R., Muthukumaraswamy, N., Pinon, D., Wu, A., Showell, H. J. & Becker, E. L. (1982) *Biochemistry* **21,** 257–263.
3. Gavuzzo, E., Lucente, G., Mazza, F., Pagani Zecchini, G., Paglialunga Paradisi, M., Pochetti, G. & Torrini, I. (1991) *Int. J. Peptide Protein Res.* **37,** 268–276.
4. Torrini, I., Pagani Zecchini, G., Paglialunga Paradisi, M., Lucente, G., Gavuzzo, E., Mazza, F., Pochetti, G., Spisani, S. & Giuliani, A. L. (1991) *Int. J. Peptide Protein Res.* **38,** 495–504.
5. Pagani Zecchini, G., Paglialunga Paradisi, M., Torrini, I., Lucente, G., Gavuzzo, E., Mazza, F., Pochetti, G. & Spisani, S. (1991) *Tetrahed. Lett.* **32,** 4375–4376.
6. Shin, C., Obara, T., Taniguchi, S. & Yonezawa, Y. (1989) *Bull. Chem. Soc. Jpn.* **62,** 1127–1135.
7. Shin, C., Yonezawa, Y. & Yamada, T. (1984) *Chem. Pharm. Bull.* **32,** 3934–3944.
8. Singh, T. P., Narula, P. & Patel, H. C. (1990) *Acta Cryst. B* **46,** 539–545.
9. Narula, P., Patel, H. C. & Singh, T. P. (1988) *Biopolymers* **27,** 1595–1606.
10. Narula, P., Patel, H. C., Singh, T. P. & Chauhan, V. S. (1990) *Biopolymers* **29,** 935–941.
11. Singh, T. P., Narula, P., Chauhan, V. S., Sharma, A. K. & Hinrichs, W. (1989) *Int. J. Peptide Protein Res.* **33,** 167–172.
12. Busetti, V., Ajò, D. & Vittadini, A. (1986) *Acta Cryst. C* **42,** 1178–1181.
13. Klyne, W. & Prelog, V. (1960) *Experientia* **16,** 521–528.
14. Ajò, D., Busetti, V. & Granozzi, G. (1982) *Tetrahedron* **38,** 3329–3334.
15. Schweizer, W. B. & Dunitz, J. D. (1982) *Helv. Chim. Acta* **65,** 1547–1554.
16. Benedetti, E., Morelli, G., Nemethy, G. & Scheraga, H. A. (1983) *Int. J. Peptide Protein Res.* **22,** 1–15.
17. Chauhan, V. S., Kaur, P., Sen, N., Uma, K., Jacob, J. & Balaram, P. (1988) *Tetrahedron* **44,** 2359–2366.
18. Bardi, R., Piazzesi, M., Toniolo, C., Ray, P. A., Ragh-

othama, S. & Balaram, P. (1986) *Int. J. Peptide Protein Res.* **27,** 229–238.
19. Wüthrich, K., Billeter, M. & Braun, W. (1984) *J. Mol. Biol.* **180,** 715–740.
20. Rao, B. N. N., Kumar, A., Balaram, H., Ravi, A. & Balaram, P. (1983) *J. Am. Chem. Soc.* **105,** 7423–7428.
21. Chauhan, V. S., Sharma, A. K., Uma, K., Paul, P. K. C. & Balaram, P. (1987) *Int. J. Peptide Protein Res.* **29,** 126–133.
22. Pardi, A., Billeter, M. & Wüthrich, K. (1984) *J. Mol. Biol.* **180,** 741–751.
23. Ashida, T., Tsunogae, Y., Tanaka, I. & Yamane, T. (1987) *Acta Cryst. B* **43,** 212–218.
24. Dentino, A. R., Raj, P. A., Bhandary, K. K., Wilson, M. E. & Levine, M. J. (1991) *J. Biol. Chem.* **266,** 18460–18468, and references cited therein.
25. Gavuzzo, E., Mazza, F., Pochetti, G. & Scatturin, A. (1989) *Int. J. Peptide Protein Res.* **34,** 409–415.
26. Becker, E. L., Bleich, H. E., Day, A. R., Freer, R. J., Glasel, J. A. & Visintainer, J. (1979) *Biochemistry* **18,** 4656–4668.
27. Iqbal, M., Balaram, P., Showell, H. J., Freer, R. J. & Becker, E. L. (1984) *FEBS Lett.* **165,** 171–174.
28. Sukumar, M., Raj, P. A., Balaram, P. & Becker, E. L. (1985) *Biochem. Biophys. Res. Commun.* **128,** 339–344.
29. Toniolo, C., Crisma, M., Valle, G., Bonora, G. M., Polinelli, S., Becker, E. L., Freer, R. J., Sudhanand, R., Balaji Rao, P., Balaram, P. & Sukumar, M. (1989) *Peptide Res.* **2,** 275–281.
30. Edmundson, A. B. & Ely, K. R. (1985) *Mol. Immunol.* **22,** 463–475.
31. Boulay, F., Tardif, M., Brouchon, L. & Vignais, P. (1990) *Biochemistry* **29,** 11123–11133.
32. Kermode, J. C., Freer, R. J. & Becker, E. L. (1991) *Biochem. J.* **276,** 715–723.
33. Kodama, H., Miyazaki, M., Kondo, M., Sakaguchi, K., Stammer, C. H. & Chen, H. C. (1992) in *Peptides Chemistry and Biology,* Smith, J. A. & Rivier, J. E., Eds., ESCOM, Leiden, pp. 423–424.
34. Main, P., Fiske, S. J., Hull, S. E., Lessinger, L., Germain, J., Declercq, J.-P. & Woolfson, M. M. (1980) *MULTAN 80. A System of Computer Programs for the Automatic Solution of Crystal Structures from X-ray Diffraction Data,* Universities of York, England, and Louvain, Belgium.
35. International Tables for X-ray Crystallography (1974) Vol. IV, Kynoch Press, Birmingham.
36. Camalli, M., Capitani, D., Cascarano, G., Cerrini, S., Giacovazzo, C. & Spagna, R. (1986) SIR-CAOS (It. pat. n. 35403c/86): *User Guide,* Istituto di Strutturistica Chimica CNR C.P. n. 10, 00016 Monterotondo Stazione, Rome.
37. Rance, M., Sorensen, O. W., Bodenhausen, G., Wagner, G., Ernst, R. R. & Wüthrich, K. (1983) *Biochem. Biophys. Res. Commun.* **117,** 479–485.
38. States, D. J., Haberkorn, R. A. & Ruben, D. J. (1982) *J. Magn. Reson.* **48,** 286–297.
39. Piantini, U., Sorensen, O. W. & Ernst R. R. (1982) *J. Am. Chem. Soc.* **104,** 6800–6801.
40. Bothner-By, A. A., Stephens, R. L., Lee, J., Warren, C. D. & Jeanloz, R. W. (1984) *J. Am. Chem. Soc.* **106,** 811–813.
41. Bax, A. & Davis, D. G. (1985) *J. Am. Chem. Soc.* **63,** 207.
42. Berendsen, H. J. C. & van Gunsteren, W. F. (1984) in *Molecular Liquids. Dynamics and Interactions,* NATO ASI Series, C135, Barnes, A. J., et al., Eds., Reidel, Dordrecht, pp. 475–500.
43. Kaptein, R., Zuiderweg, E. R. P., Scheek, R. M., Boelens, R. & van Gunsteren, W. F. (1985) *J. Mol. Biol.* **182,** 179–182.
44. Aqvist, J., van Gunsteren, W. F., Leijonmarck, M. & Tapia, O. (1985) *J. Mol. Biol.* **183,** 461–477.
45. Kaptein, R., Boelens, R., Scheek, R. M. & van Gunsteren, W. F. (1988) *Biochemistry* **27,** 5389–5395.
46. Ryckaert, J. P., Ciccotti, G. & Berendsen, H. J. C. (1977) *J. Comput. Phys.* **23,** 327–341.
47. Berendsen, H. J. C., Postma, J. P. M., van Gunsteren, W. F., Di Nola, A. & Haak, J. R. (1984) *J. Chem. Phys.* **81,** 3684–3690.
48. Zigmond, S. H. & Hirsch, J. G. (1973) *J. Exp. Med.* **137,** 387–391.
49. Spisani, S., Cavalletti, T., Gavioli, R., Scatturin, A., Vertuani, G. & Traniello, S. (1986) *Inflammation* **10,** 363–369.

Received April 22, 1992
Accepted August 27, 1992